Hindawi Publishing Corporation
Journal of Nanomaterials
Volume 2014, Article ID 452468, 7 pages
http://dx.doi.org/10.1155/2014/452468

Research Article

Enhanced Magnetization of Sol-Gel Synthesized Pb-Doped Strontium Hexaferrites Nanocrystallites at Low Temperature

Shahid M. Ramay,[1] Shahid Atiq,[2] Murtaza Saleem,[3] Asif Mahmood,[4] Saadat A. Siddiqi,[5] Shahzad Naseem,[2] Yousef Al-Zeghayer,[4,6] Nasser S. Alzayed,[1] and Mohammed Shahabuddin[1]

[1] *Department of Physics and Astronomy, College of Science, King Saud University, P.O. Box 800, Riyadh 11421, Saudi Arabia*
[2] *Centre of Excellence in Solid State Physics, University of the Punjab, Lahore 54590, Pakistan*
[3] *Department of Physics, School of Science and Engineering (SSE), Lahore University of Management Sciences (LUMS), Lahore 54792, Pakistan*
[4] *Department of Chemical Engineering, College of Engineering, King Saud University, P.O. Box 800, Riyadh 11421, Saudi Arabia*
[5] *Interdisciplinary Research Centre in Biomedical Materials (IRCBM), COMSATS Institute of Information Technology, Defence Road, Off Raiwind Road, Lahore 54600, Pakistan*
[6] *Industrial Catalysts Research Chair, King Saud University, Riyadh 11421, Saudi Arabia*

Correspondence should be addressed to Shahid Atiq; satiq.cssp@pu.edu.pk

Received 24 January 2014; Revised 1 May 2014; Accepted 3 May 2014; Published 27 May 2014

Academic Editor: Debasis Dhak

Effect of Pb doping on the structural and low temperature magnetic properties of $SrPb_xFe_{12-x}O_{19}$ ($x = 0, 0.1, 0.2, 0.3,$ and 0.4), synthesized by sol-gel autocombustion technique, has been investigated. The powder samples were sintered at 800°C for 2 h in order to develop the stable hexagonal phase, characteristic of the $SrFe_{12}O_{19}$ structure. The consequences of Pb substitution (at iron sites) on various structural parameters like lattice constants, unit cell volume, crystallite size, and porosity have been discussed. Fourier transform infrared frequency bands were utilized to determine the formation of tetrahedral and octahedral clusters of M-type ferrites. Hexagonal texture of the grains, a characteristic of the hexagonal crystal structure of $SrFe_{12}O_{19}$, was refined by Pb substitution. The magnetic properties, determined using a vibrating sample magnetometer, revealed that saturation magnetization decreased, while coercivity was increased with the increase of Pb contents. However, the increased squareness ratio and hence the energy product motivate the utilization of these ferrite compositions where hard magnetic characteristics are required. The increased values of saturation magnetization were observed at reduced temperature of 200 K, attributable to the better spin alignments of individual magnetic moments at low temperature.

1. Introduction

M-type hexagonal ferrites belong to immensely valuable class of magnetic materials, with a host of applications ranging from simple permanent magnets used in electric motors to modern day applications, for instance, as radar wave absorbing materials. Owing to its high values of saturation magnetization and coercivity [1], strontium hexaferrite, in particular, is a very important member of this class of magnetic materials, being widely used in telecommunication [2], magnetooptic recording media, microwave devices [3], and electronic industry [4]. Various preparation techniques like coprecipitation process, molten salt method, solid state reaction method [5], double sintering ceramic technique [6], microwave-induced combustion process, sol-gel based synthesis routes [7], and so forth have been adopted by the researchers to refine the astonishing structural and magnetic properties of these ferrites. However, sol-gel based autocombustion route, being easier, energy efficient, and cheaper, has emerged as a novel technique to prepare single phase strontium hexaferrites. The crystal structure of $SrFe_{12}O_{19}$ is hexagonal which has a great influence on valuable characteristics of these ferrites. One-unit cell of these ferrites is composed of 64 ions that are distributed in such a way that

these form two formula units, each having one spinel S-block and one hexagonal R-block [2]. The Fe^{3+} ions are oriented on five different crystallographic sites in the unit cell. These ions are the major cause of magnetism in these ferrites, resulting in net magnetic moment of 20 μ_B per formula unit [8, 9].

Ferrimagnetic strontium hexaferrites are n-type semiconductor with band gap energy of 0.6 eV. Researchers are attempting to improve the intrinsic properties of these ferrites for innovations. For this purpose, introduction of some divalent or trivalent dopant element and optimization of preparation technique play a vital role. Diamagnetic Pb ions, substituted at Fe sites with spin up, could enhance the hard magnetic characteristics of $SrFe_{12}O_{19}$ when doped stoichiometrically. Hence, it has been understood as a quite suitable dopant choice for these ferrites to improve not only the structural properties but also the magnetic properties [2, 3, 8]. In the present work, we have successfully employed sol-gel based autocombustion technique to prepare the ferrite samples in phase-pure form to investigate the structural and low temperature magnetic properties of Pb-doped strontium hexaferrites for use in devices that work efficiently with high values of coercivity and electrical devices that show minimum energy losses at higher applied frequencies.

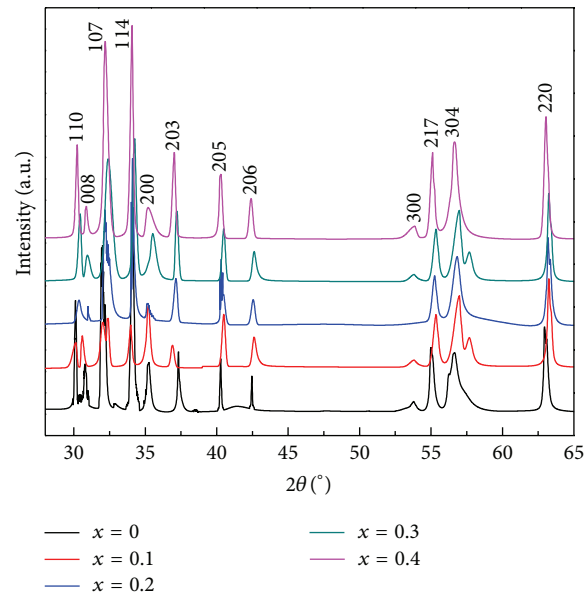

FIGURE 1: X-ray diffraction patterns of $SrPb_xFe_{12-x}O_{19}$ ($x = 0.0, 0.1, 0.2, 0.3,$ and 0.4) sample.

2. Experimental

Single phase polycrystalline samples with compositions $SrPb_xFe_{12-x}O_{19}$ ($x = 0.0, 0.1, 0.2, 0.3,$ and 0.4) were prepared by a novel sol-gel based autocombustion route. A transparent homogenous solution was obtained by dissolving stoichiometric proportions of analytical grade strontium nitrate (Sigma Aldrich), iron (III) nitrate (Sigma Aldrich), lead (II) nitrate (Sigma Aldrich), and citric acid (Avonchem, UK) in 50 mL of deionized water. The relative molar concentrations of citric acid, used as a fuel, and metal nitrates were in the ratio of 2 : 1. The solution was placed over a hot plate, positioned in a fume hood. The temperature of the hot plate was gradually increased to 90°C. The solution was continuously stirred using a magnetic stirrer at 500 rpm, for about 1 h, until it converted into a soft gel. At that instance, the rotator was stopped and the stirrer was removed from the gel. The temperature of the gel was increased in steps up to 300°C. As the gel was heated at this temperature for about 15 min., it burnt suddenly and vigorously and converted into soft and fluffy powder. The product was grinded to get homogenously mixed powder samples. All the samples were synthesized using the same procedure and sintered at 800°C for 2 h in order to get hexagonal ferrite phases. X-ray diffraction (XRD) was used to investigate the crystal structure of the prepared samples. The thermogravimetric/differential (TG/DTA) analysis was performed using EXSTAR SII TG/DTA 7300 analyzer in order to investigate any weight loss of the samples at high temperatures. The powder samples were then pelletized and surface morphology was analyzed using a JSM-6610 Oxford (with EDX attachment) scanning electron microscope (SEM). Energy dispersive X-ray spectroscopy (EDX) was performed to get quantitative analysis of the samples. The formation of chemical bonds in the desired crystal phase was confirmed by Fourier transform infrared spectroscopy (FTIR). Magnetic behavior of the samples was analyzed using a 14 Tesla Quantum design PPMS (Physical Properties Measurement System).

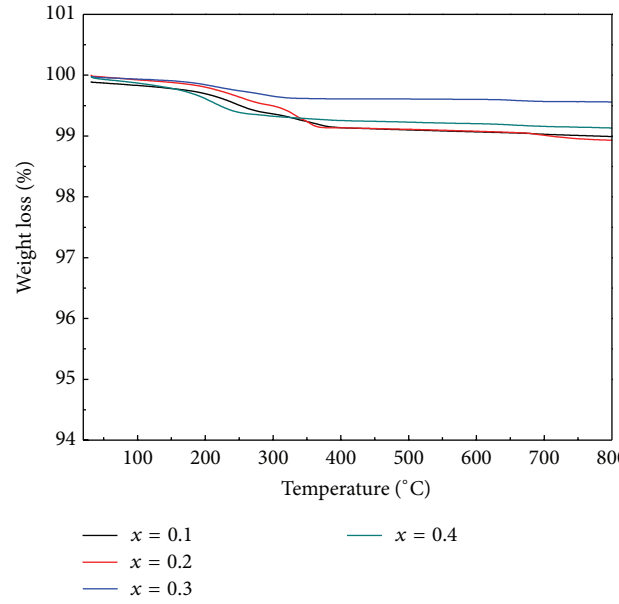

FIGURE 2: TGA spectra of $SrPb_xFe_{12-x}O_{19}$ ($x = 0.1, 0.2, 0.3,$ and 0.4) samples.

3. Results and Discussion

Crystal structure of all the prepared samples was determined by X-ray diffraction, following the complete procedure as

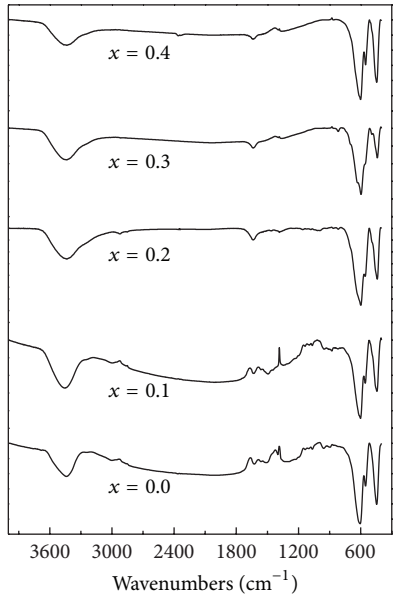

Figure 3: FTIR spectra of $SrPb_xFe_{12-x}O_{19}$ ($x = 0.0, 0.1, 0.2, 0.3,$ and 0.4) samples.

described by Cullity [10]. Data obtained from the diffractometer was plotted. Positions of the diffracted intensities were noted and corresponding values of $\sin^2\theta$ were evaluated. These values were multiplied by 1/3, 1/4, and 1/7 in order to find a repeated number named "A" related to the lattice parameter "a" and wavelength (λ) of the incident radiation by the relation $A = \lambda^2/3a^2$. Using this relation, value of "a" was evaluated for 200 plane. The relation $\sin^2\theta - A(h^2 + hk + k^2) = Cl^2$ was used to find a parameter, "C" and hence the lattice constant, "c," using the expression $C = \lambda^2/4c^2$. hkl values corresponding to all the diffracted intensities were determined and the patterns were indexed as shown in Figure 1. The indexing of the patterns revealed that crystal structures of all the samples exhibit characteristic hexagonal structure. In addition, the indexed peaks were also matched with the standard data (ICSD-00-033-1340), which confirmed that samples revealing hexagonal structure consisted of M-type strontium hexaferrites. TGA was performed up to 800°C with a heating rate of 20°C/min. to determine any carbon related species that may be present in the samples due to reaction of Sr^{2+} with CO_2 which may be available from the atmosphere and/or from the decomposition of citric acid. Figure 2 shows the %age weight loss for the four samples from room temperature to 800°C. The curves reveal a good stability and do not indicate any significant weight loss. Hence, it is inferred that no carbon related species are present in the prepared samples and sintering of samples at 800°C is sufficient to hinder the formation of $SrCO_3$ enabling the Sr^{2+} available to stimulate the incorporation of Sr^{2+} into strontium hexaferrite matrix [11]. Slight increase in the lattice parameters "a" and "c" was observed that led to a minute increase in the unit cell volume ($V = 0.866a^2c$) as well. The trend might be attributed to the larger ionic radius of the substituent, Pb^{2+} (0.98 Å) as compared to the host, Fe^{3+} (0.49 Å). The crystallite sizes of all the samples evaluated using Scherrer's relation ($D = k\lambda/\beta cos\theta$, k is a constant, β is full width at half maximum in radians, and θ is diffraction angle in degrees) were increased slightly as the Pb concentration was increased in the series. The bulk density (ρ_b) was calculated from the weight and dimensions of the sintered pellets using the relation $\rho_b = m/\pi r^2 h$, where m is the mass, r is the radius, and h is the thickness of the samples. X-ray density (ρ_x) of the samples was calculated using the relation $\rho_x = 2M/N_a a^3$ [12], where M is the molecular weight of the composition, N_a is Avogadro's number, and a is the lattice constant. The bulk and X-ray densities were used to calculate the porosity ($P = 1 - \rho_b/\rho_x$). The values of all these structural parameters have been shown in Table 1. The results reveal that porosity of the samples was decreased as the Pb contents were substituted at the Fe sites in the series of the samples. In other words, the grains became more compact and densified with the Pb substitution which could play a significant role in establishing the structural and magnetic properties.

Table 1: Values of lattice constants, their axial ratio, unit cell volume (V), crystallite size (D), bulk density (ρ_b), X-ray density (ρ_x), porosity (P), saturation magnetization (M_s), remanence (M_r), M_r/M_s, and coercivity (H_c) at $SrPb_xFe_{12-x}O_{19}$ ($x = 0.0, 0.1, 0.2, 0.3,$ and 0.4).

Parameter	$x = 0.0$	$x = 0.1$	$x = 0.2$	$x = 0.3$	$x = 0.4$
a (Å)	5.8808	5.8856	5.8880	5.8889	5.8911
c (Å)	23.2018	23.2193	23.2297	23.2360	23.2361
c/a	3.9453	3.9451	3.9446	3.9457	3.9443
V (nm^3)	694.8841	696.5439	697.3042	697.8268	698.3515
D (nm)	27.8971	28.4145	28.8917	29.9115	29.9176
ρ_b (g/cm^3)	2.9124	2.9965	3.1623	3.2817	3.2862
ρ_x (g/cm^3)	4.8167	4.8266	4.8615	4.9075	4.9080
P (%)	39.53	37.92	34.95	33.13	33.04
M_s (emu/g) at 300 K	63.22	57.79	53.16	49.65	41.62
M_s (emu/g) at 200 K	70.77	63.50	60.50	53.93	48.44
M_r (emu/g) at 300 K	33.05	30.62	28.71	25.84	23.66
M_r (emu/g) at 200 K	38.20	34.81	33.65	30.96	28.84
M_r/M_s at 300 K	0.52	0.53	0.54	0.55	0.57
M_r/M_s at 200 K	0.54	0.55	0.56	0.58	0.60
H_c (Oe) at 300 K	2360	3249	4360	5837	6015
H_c (Oe) at 200 K	3104	3471	4322	4915	5282

Figure 3 shows the FTIR spectra of all the prepared samples. In ferrites, the spectroscopically active region lies between 400 cm^{-1} and 800 cm^{-1} [13]. In our samples, there were sharp and clear peaks at 600 cm^{-1}, 550 cm^{-1}, and 440 cm^{-1}, corresponding to the characteristics peaks of chemical bonds in $SrFe_{12}O_{19}$ structure [14]. The peak intensity remained almost the same as the amount that Pb dopant

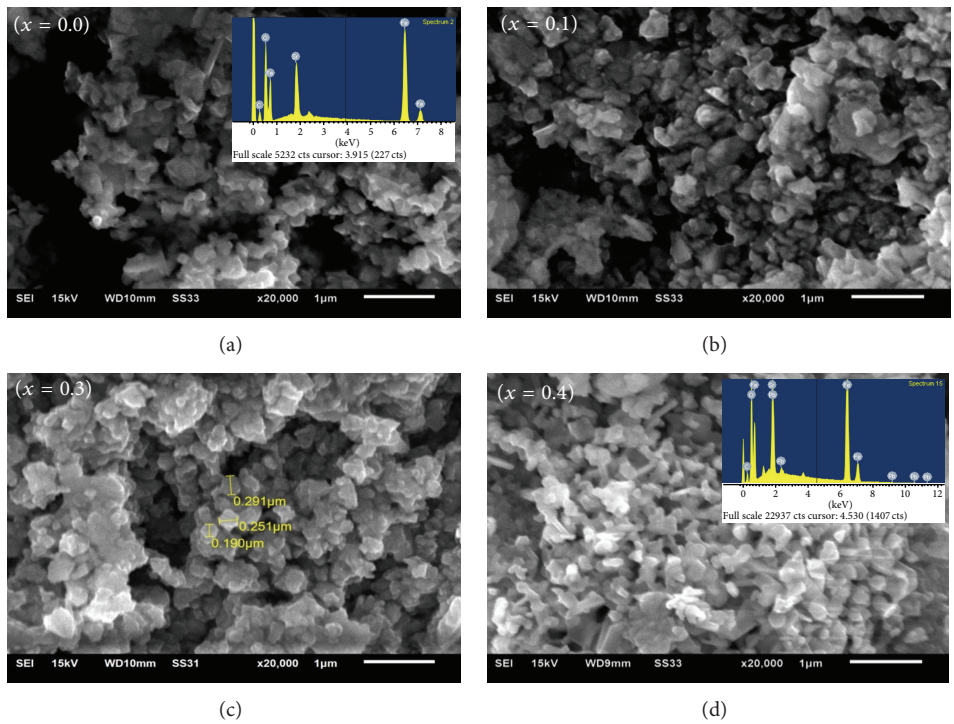

FIGURE 4: SEM micrographs of $SrPb_xFe_{12-x}O_{19}$ ($x = 0.0, 0.1, 0.3,$ and 0.4) samples.

was increased by in the series, which indicated that Pb could be successfully substituted in a dilute amount at the Fe sites, without disturbing the stoichiometry of the parent hexagonal $SrFe_{12}O_{19}$ structure. With the increase in Pb contents, the chemical polarization of the internal bonds could be shared in the form of Fe-O-Pb and Sr-O-Pb chemical bonds, resulting in compact structures as that of $SrFe_{12}O_{19}$. The peaks at 3421 cm^{-1} and 1639 cm^{-1} exhibit the structure and bending bonds of the surface hydrogen group (–OH) earned from the damped environment [15].

Figure 4 shows the microstructural morphology of the samples obtained using a scanning electron microscope. Figure 4(a) reveals the micrograph of pure $SrFe_{12}O_{19}$ sample indicating that most of the grains are like platelets having sharp grain boundaries. A close look at this image might provide hindsight of the hexagonal texture of the grains, a characteristic of the hexagonal crystal structure of the $SrFe_{12}O_{19}$. With the substitution of Pb contents at Fe sites, the microstructural morphology of the grains was further refined until at $x = 0.3$ Pb contents; well defined hexagonal grains were witnessed which were varying in size ranging from 0.190 to 0.291 μm. The uniform grain sizes and homogeneous contrast throughout the focused area confirm that the sample consists of single phase ferrite composition. The shape and compatibility of grains play a vital role in determining the structural and magnetic properties of ferrites [16]. The platelet-like hexagonal texture of ferrites has been investigated as a potential candidate for use in microwave absorbing coatings [17]. The elemental composition of the constituents elicited from EDX, shown in the inset of Figures 4(a) and 4(d), confirms the stoichiometric ratio of the elements in the prepared samples and the incorporation of Pb at Fe sites. The quantitative data of atomic and percentage composition of elements was in close agreement with the dissolved reactants.

Figure 5 shows the magnetic-hysteresis (M-H) loops of the prepared samples obtained at 300 K. Magnetic parameters like saturation magnetization (M_s), remanence (M_r), and coercivity (H_c) were determined from M-H loops as listed in Table 1. The M_s and H_c values as a function of Pb contents have been plotted in Figure 6. The plots reveal that the substitution of Pb contents at A-site of Fe changes the magnetic properties of the ferrite samples in a remarkable way. The M_s and M_r values of the ferrite samples were decreased from 63.22 to 41.62 emu/g and 33.03 to 23.66 emu/g, respectively, whereas the H_c value was increased from 2360 to 6015 Oe with the increase in the Pb contents. However, the M_r/M_s ratio was observed to increase from 0.52 to 0.57 in the series, as the decrease in M_r value is less prominent as the corresponding decrease in the M_s value, making the later samples in the series more effective, as far as energy product is concerned. The value of M_s at $x = 0$ is in close agreement with a recently reported value [18]. The crystal structure has been understood as a critical factor which decides the magnetic behavior of the material. The crystal structure of $SrFe_{12}O_{19}$ has five nonequivalent sublattices with three octahedral (2a, 12k, and 4f), one tetrahedral (4f1), and one trigonal bipyramidal (2b) sites [19]. Among these, three sites (2a, 12k, and 2b) possess upward spin and two sites (4f1 and 4f2) spin downward. Hence, net magnetic moment results due to upward spins. When Pb with a diamagnetic nature is substituted with some of the iron ions, a decrease in the net saturation magnetization is observed which decreases

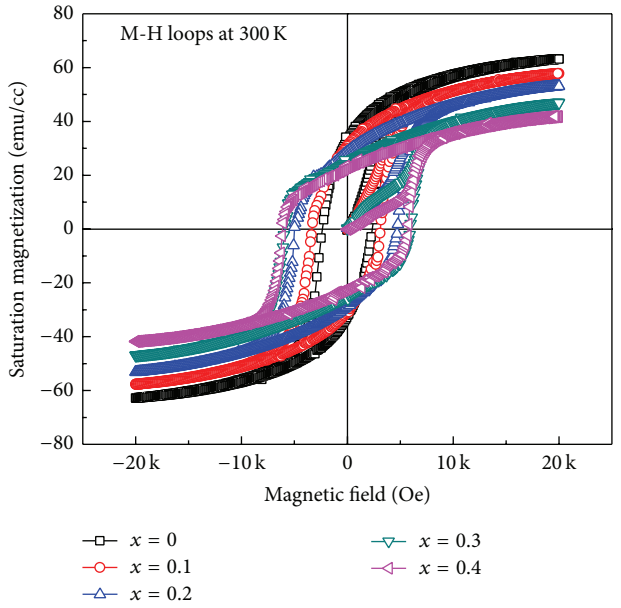

FIGURE 5: M-H loops of $SrPb_xFe_{12-x}O_{19}$ ($x = 0.0, 0.1, 0.2, 0.3,$ and 0.4) samples at 300 K.

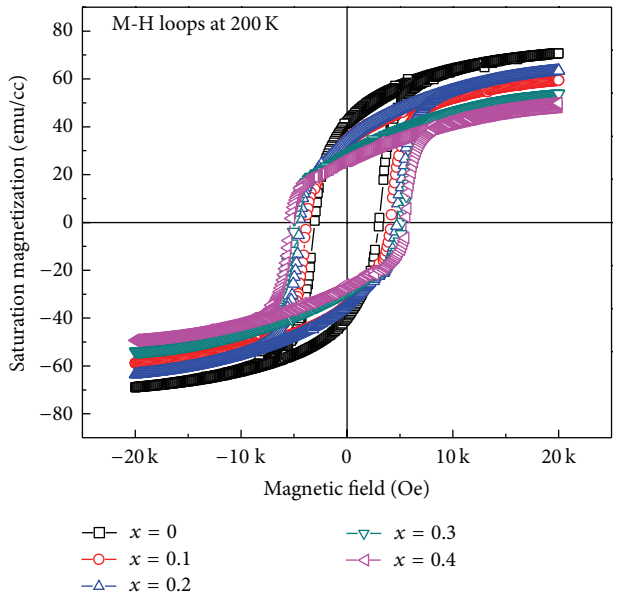

FIGURE 7: M-H loops of $SrPb_xFe_{12-x}O_{19}$ ($x = 0.0, 0.1, 0.2, 0.3,$ and 0.4) samples at 200 K.

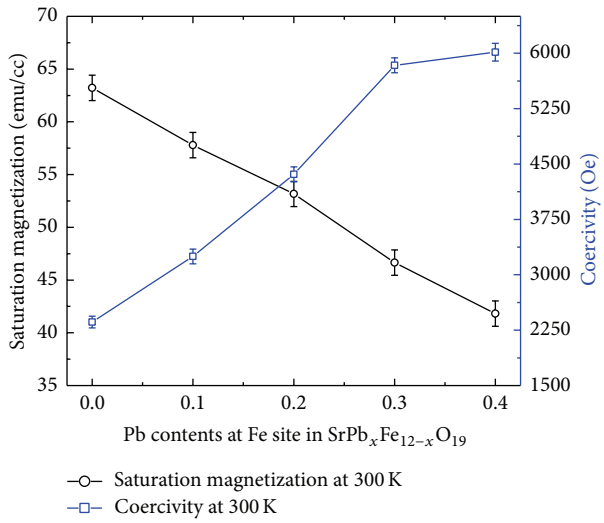

FIGURE 6: M_s and H_c as a function of Pb contents at Fe sites in $SrPb_xFe_{12-x}O_{19}$ at 300 K.

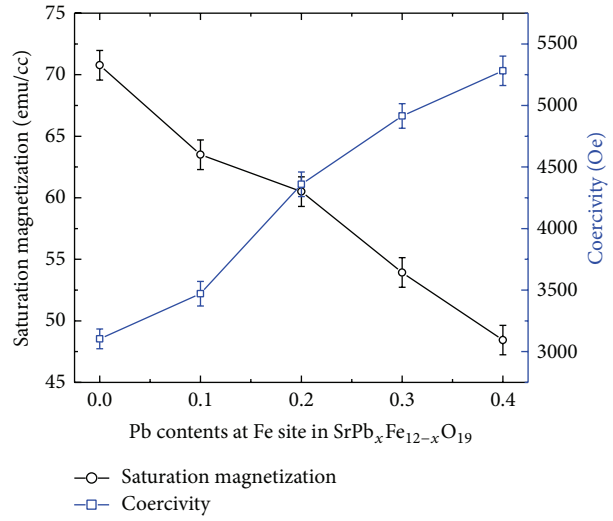

FIGURE 8: M_s and H_c as a function of Pb contents at Fe sites in $SrPb_xFe_{12-x}O_{19}$ at 200 K.

further as the Pb contents are increased up to $x = 0.4$. This decrease in M_s value could be attributed to the decrease of superexchange interactions among Fe_A^{3+}-O-Fe_B^{3+}, as the substituted ions prefer to occupy the octahedral 12k site which has upward spin [20], followed by 2a and 4f2 sites [19]. Each Fe^{3+} ion possesses a magnetic moment of 5 μ_B. Therefore, an M-type molecule of $SrFe_{12}O_{19}$ possesses a magnetic moment of 20.6 μ_B. The substitution of a diamagnetic ion at a site with spin up reduces the total magnetic moment of the specimen and hence the M_s values decrease.

The increase in H_c with the increase in Pb contents may be described on the basis of Stoner-Wohlfarth relation, $H_c = 2K/\mu_o M_s$, where K is magnetocrystalline anisotropy and μ_o is permittivity of free space ($= 4\pi \times 10^{-7}$ H/m). Hence, a decrease in M_s and an increase in K [21] are the possible factors for an increased value of H_c.

Figure 7 shows the M-H loops of the samples at 200 K. The M_s and M_r values of all the samples increased as compared to their corresponding values at 300 K in the series, with the decrease in temperature, as has been plotted in Figure 8 and listed in Table 1, but decreased with the increase of Pb contents in the series. The increase in H_c as a function of Pb contents at 200 K (Figure 7) could also be explained as discussed earlier. The increased values of M_s at 200 K might be described on the basis of Weiss theory of ferromagnetism

[22]. According to this theory, at low temperatures, the thermal activation energy of the magnetic ions reduces which in turn helps the magnetic moments to align more easily in the applied field direction. Therefore, an overall increase in the magnetic moment and hence in the M_s is observed. The increased squareness ratio (M_r/M_s) in this case as well favors the use of these materials for the applications where high energy products are desired.

4. Conclusion

In this paper, the influence of Pb doping on the structural and low temperature magnetic behavior of $SrPb_xFe_{12-x}O_{19}$ (x = 0, 0.1, 0.2, 0.3, and 0.4) has been investigated systematically. X-ray diffraction analysis of all the samples revealed the hexagonal phase characteristics of the $SrFe_{12}O_{19}$ crystal structure. A slight increase in the lattice constants (a and c) and the unit cell volume was attributed to the larger ionic radii of dopant Pb as compared to the host Fe site. The crystallite size was also increased in the series as the Pb contents were increased. The porosity was decreased from 39.53 to 33.04% in the series making the samples more compact to improve the structural and hence the magnetic properties. FTIR spectroscopy confirmed the metal-oxygen bonds formation in the hexagonal structure of the samples. Surface morphology has been described using SEM images and elemental stoichiometric composition has been found using EDX spectroscopy. Saturation magnetization was found to decrease, while coercivity was increased with the increase of Pb contents in the series at 300 K. When temperature was reduced to 200 K, the saturation magnetization of the relevant samples was increased, credited to the preferred individual spin alignments at low temperature. Remanence was also decreased, but the corresponding effect was less prominent as the M_r/M_s and consequently the energy product was found to increase, corroborating the use of these ferrite compositions where hard magnetic characteristics are required.

Conflict of Interests

The authors declare that they have no conflict of interests regarding the publication of this paper.

Acknowledgment

The authors extend their appreciation to the Deanship of Scientific Research at King Saud University for funding the work through the research group project no. RGP-VPP-106.

References

[1] Y.-P. Fu and C.-H. Lin, "Fe/Sr ratio effect on magnetic properties of strontium ferrite powders synthesized by microwave-induced combustion process," *Journal of Alloys and Compounds*, vol. 386, no. 1-2, pp. 222–227, 2005.

[2] Z. Ullah, S. Atiq, and S. Naseem, "Influence of Pb doping on structural, electrical and magnetic properties of Sr-hexaferrites," *Journal of Alloys and Compounds*, vol. 555, pp. 263–267, 2013.

[3] I. V. Zavislyak, M. A. Popov, and G. Srinivasan, "A cut-off millimeter wave resonator technique for mapping magnetic parameters in hexagonal ferrites," *Measurement Science and Technology*, vol. 20, no. 11, Article ID 115704, 2009.

[4] S. Hussain and A. Maqsood, "Structural and electrical properties of Pb-doped Sr-hexa ferrites," *Journal of Alloys and Compounds*, vol. 466, no. 1-2, pp. 293–298, 2008.

[5] S.-D. Kim and J.-S. Kim, "Magnetic properties of Sr-ferrites synthesized in molten (NaCl + KCl) flux," *Journal of Magnetism and Magnetic Materials*, vol. 307, no. 2, pp. 295–300, 2006.

[6] S. Hussain and A. Maqsood, "Thermal transport properties of silica added Sr-hexa ferrites as a function of temperature," *Materials Letters*, vol. 62, no. 6-7, pp. 1002–1005, 2008.

[7] L. You, L. Qiao, J. Zheng, M. Jiang, L. Jiang, and J. Sheng, "Magnetic properties of La-Zn substituted Sr-hexaferrites by self-propagation high-temperature synthesis," *Journal of Rare Earths*, vol. 26, no. 1, pp. 81–84, 2008.

[8] M. J. Iqbal and S. Farooq, "Extraordinary role of Ce-Ni elements on the electrical and magnetic properties of Sr-Ba M-type hexaferrites," *Materials Research Bulletin*, vol. 44, no. 11, pp. 2050–2055, 2009.

[9] C. M. Fang, F. Kools, R. Metselaar, G. De With, and R. A. De Groot, "Magnetic and electronic properties of strontium hexaferrite $SrFe_{12}O_{19}$ from first-principles calculations," *Journal of Physics Condensed Matter*, vol. 15, no. 36, pp. 6229–6237, 2003.

[10] B. D. Cullity, *Elements of X-Ray Diffraction*, Addison-Wesley, 2nd edition, 1978.

[11] R. M. Garcia, E. R. Ruiz, and E. E. Rams, "Structural characterization of low temperature synthesized $SrFe_{12}O_{19}$," *Materials Letters*, vol. 50, no. 2-3, pp. 183–187, 2001.

[12] J. Smit and H. P. J. Wijn, *Ferrites*, John Wiley & Sons, New York, NY, USA, 1959.

[13] X. Yang, Q. Li, J. Zhao, B. Li, and Y. Wang, "Preparation and magnetic properties of controllable-morphologies nano-$SrFe_{12}O_{19}$ particles prepared by sol-gel self-propagation synthesis," *Journal of Alloys and Compounds*, vol. 475, no. 1-2, pp. 312–315, 2009.

[14] T. Xie, L. Xu, and C. Liu, "Synthesis and properties of composite magnetic material $SrCo_xFe_{12-x}O_{19}$ (x = 0-0.3)," *Powder Technology*, vol. 232, pp. 87–92, 2012.

[15] S. Kong, P. Zhang, X. Wen et al., "Influence of surface modification of $SrFe_{12}O_{19}$ particles with oleic acid on magnetic microsphere preparation," *Particuology*, vol. 6, no. 3, pp. 185–190, 2008.

[16] M. Ahmad, R. Grossinger, M. Kriegisch, F. Kubel, and M. U. Rana, "Characterization of Sr-substituted W-type hexagonal ferrites synthesized by sol-gel autocombustion method," *Journal of Magnetism and Magnetic Materials*, vol. 332, pp. 137–145, 2013.

[17] J. Xu, H. Zou, H. Li, G. Li, S. Gan, and G. Hong, "Influence of Nd3+ substitution on the microstructure and electromagnetic properties of barium W-type hexaferrite," *Journal of Alloys and Compounds*, vol. 490, no. 1-2, pp. 552–556, 2010.

[18] F. S. Jesus, A. M. Bolarin-Miro, C. A. Cortes-Escobedo, R. Valenzuela, and S. Ammar, "Mechanosynthesis, crystal structure and magnetic characterization of M-type $SrFe_{12}O_{19}$," *Ceramics International*, vol. 40, no. 3, pp. 4033–4038, 2014.

[19] S. Singhal, T. Namgyal, J. Singh, K. Chandra, and S. Bansal, "A comparative study on the magnetic properties of $MFe_{12}O_{19}$ and $MAlFe_{11}O_{19}$ (M = Sr, Ba and Pb) hexaferrites with different morphologies," *Ceramics International*, vol. 37, no. 6, pp. 1833–1837, 2011.

[20] M. J. Iqbal, M. N. Ashiq, P. Hernandez-Gomez, and J. M. Munoz, "Synthesis, physical, magnetic and electrical properties of Al-Ga substituted co-precipitated nanocrystalline strontium hexaferrite," *Journal of Magnetism and Magnetic Materials*, vol. 320, no. 6, pp. 881–886, 2008.

[21] D. Y. Chen, Y. Y. Meng, D. C. Zeng, Z. W. Liu, H. Y. Yu, and X. C. Zhong, "CTAB-assisted low-temperature synthesis of $SrFe_{12}O_{19}$ ultrathin hexagonal platelets and its formation mechanism," *Materials Letters*, vol. 76, pp. 84–86, 2012.

[22] P. Weiss, "L'hypothèse du champ moléculaire et la propriété ferromagnétique," *Journal of Physics, Theory Applications*, vol. 6, no. 4, pp. 661–690, 1907.